Experimental Study of Dynamic Wetting in Reverse-Roll Coating

H. Benkreira
Dept. of Chemical Engineering, University of Bradford, BD7 1DP, Bradford, UK

The movement of the dynamic wetting line in reverse-roll coating was followed in a series of experiments that gave position, X_D, angle, θ_D and the critical metering roller speed, $V_{M,\ cascade}$, for the onset of cascade. The data were correlated with operating conditions and compared with plunging-tape air-entrainment speeds, $V^*_{plunging}$. It was found that there was hydrodynamic assistance of wetting similar in form but smaller in magnitude to that reported in curtain coating. The correlated data for X_D and θ_D also provide boundary conditions, which can replace the assumptions usually made in the simulations of reverse-roll coating flows.

Introduction

Dynamic wetting is an integral feature of all coating processes, and occurs at the line where a thin liquid film displaces air in contact with a moving dry solid substrate. Dynamic wetting failure results in air entrainment, which is a serious limitation to good and fast coating. The study of dynamic wetting in coating flows has been based largely on plunging-tape experiments, where a substrate or a scraped rotating cylinder surface is plunged into a large pool of liquid. At low substrate speeds the wetting line is straight and the corresponding dynamic contact angle θ_D is not much larger than the static contact angle, θ_S. As the speed of the substrate is increased, the wetting line advances in the direction of flow, causing θ_D to increase until, at a critical speed, V^*_{plunging}, it approaches 180°. At this point dynamic wetting failure occurs; the wetting line becomes unsteady and breaks into segments. At speeds greater than V^*_{plunging}, air is entrained in the form of fine bubbles detaching from the tips of the segments.

The data of Deryagin and Levi (1964), Perry (1967), Inverarity (1969), Schwartz and Tejada (1972), Burley and Kennedy (1976), Gutoff and Kendrick (1982), Burley and Jolly (1984), Bracke et al. (1989), and Blake and Ruschak (1997) all show that the main controlling parameter of θ_D is the capillary number $Ca = \mu V/\sigma$. They all found θ_D to be an increasing S-shaped function of Ca from θ_s to 180°. Initially the angle increases sharply with speed; it then approaches 180° more gradually. Similar observations have been made in capillary flows by Blake and Haynes (1969), Hoffman (1975), and Rillaerts and Joos (1980), and in drop-spreading flows by Dussan (1979). There are, however, significant differences in the quantitative correlations between θ_D and Ca, because Ca alone cannot describe all the events very near the solid surface where molecular considerations must play a part. As yet there is no universally agreed theoretical or experimental correlation for θ_D. Figure 1 gives a summary of the data for the plunging-tape flow and highlights this disparity. As for the more practical coating operations, such as metering forward-, reverse-, gravure- or deformable-roll coating or premetered die and curtain coating, no data for θ_D are available. This information is crucial for mathematical modeling, which at present fixes θ_D arbitrarily (Coyle et al., 1990). One objective of this article is to present θ_D data for reverse-roll coating, the most common coating flow.

The same studies cited earlier found that V^*_{plunging} of smooth substrates is controlled essentially by viscosity. [Note that substrate roughness (Buonoplane et al., 1986) and wetting angle (Cohu and Benkreira, 1998) postpone air entrainment to significantly higher speeds.] It has an upper limit of about 0.1 m/s for fluids of $\mu \geq 0.5$ Pa·s (Burley and Kennedy, 1976) and it is proportional to $\mu^{-0.67 \rightarrow -0.87}$ when $\mu < 0.5$ Pa·s. A typical and often-quoted correlation is that due to Gutoff and Kendrick (1982)

$$V^*_{\text{plunging}} = 0.05\mu^{-0.67} \tag{1}$$

where V^*_{plunging} is expressed in m/s and μ in Pa·s. Gutoff and Kendrick (1982) also found that the air-entrainment speed in slide coating and slot coating is similar to that in the plunging-tape flow. Such a result confirms the fundamental

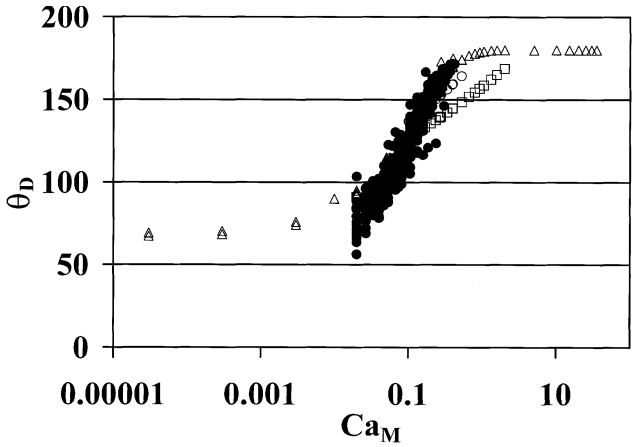

Figure 1. θ_D vs. Ca_M from this study (•) vs. other data.

△: Blake and Ruschak, 1997; Hoffman, 1975; Rillaerts and Joos, 1980; ○: Burley and Kennedy, □: Esmail and Ghannam, 1990).

basis of plunging-tape experiments in unraveling the mechanism of dynamic wetting and air entrainment in coating flows, but only for situations where the hydrodynamic and capillary forces are small and comparable (Blake and Ruschak, 1997).

By studying air entrainment in curtain coating, Blake et al. (1994) considered a coating flow where hydrodynamic effects are much larger than in plunging-tape, slot or slide coating. These authors showed experimentally that under conditions where the wetting line is located beneath the curtain, the pressure generated by the impact of the liquid on the substrate assists dynamic wetting and postpones air entrainment to much higher (10 times faster) velocities V^*_{curtain}. Effectively, the controlling parameter is the characteristic speed, U of the liquid impinging on the wetting line. Blake et al. (1994) found that V^*_{curtain} also correlates with viscosity, but to a lesser extent than in plunging-tape flow

$$V^*_{curtain} = 2.46U^{0.66}\mu^{-0.17} \tag{2}$$

This agrees with the argument that at critical conditions, the force dragging the wetting line must just balance the force pinning it, which Blake et al. (1994) equate to

$$V^*_{curtain} = 2.18U^{0.871}\mu^{-0.19} \tag{3}$$

Curtain coating, however, is not the only example of a hydrodynamically controlled type of flow, nor is it the most common coating arrangement. Metered coatings flows such as roll coating are more commonly used. They include forward- and reverse-roll coating with rigid, deformable, or gravure rollers. In all these flows, hydrodynamic effects can be large with the geometry of the small coating gaps and the high roller speeds. Unlike for curtain coating, hydrodynamic assistance in reverse-roll coating has not been established. This forms the second objective of this article.

Figure 2 illustrates the reverse-roll-coating flow variables: the metering gap, H_0, the applicator roller speed, V_A, and the metering roller speed, V_M. Previous related research was

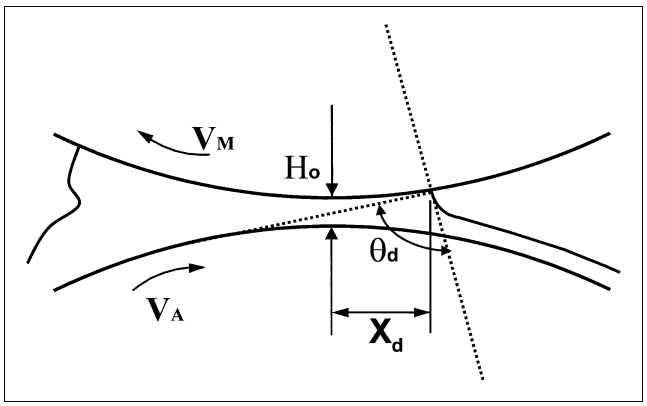

Figure 2. Reverse-roll-coating flow arrangement.

presented by Coyle et al. (1990). They observed an air instability in the form of large air bubbles being engulfed, which they describe as a cascade. This cascade occurs, for a given applicator roll capillary number Ca_A ($= \mu V_A/\sigma$), at critical speed ratio S_{cascade} ($= V_{M,\text{ cascade}}/V_A$) when

$$Ca_A = 0.16S^{-2.16}_{\text{cascade}} \quad \text{or} \quad S_{\text{cascade}} = 0.43\,Ca_A^{-0.46} \tag{4}$$

The cascade they describe is "closely associated with the events near the dynamic wetting line" and "a mode of air entrainment completely different from the high speed mode observed in plunging tape experiment and curtain coating." In a subsequent republication of these results, Coyle (1997) links the onset of cascade to the conditions minimizing the metered film thickness observed by Kang and Liu (1991) as

$$Ca_A = 0.105\left[V_{M,X_D=0/V_A}\right]^{-1.82} \text{ or } V_{M,X_D=0}/V_A = 0.29Ca_A^{-0.55} \tag{5}$$

The link between the correlations is attributed to the movement of the wetting line to the gap position, that is, with reference to Figure 2, at $X_D = 0$. In the words of Coyle (1997), "the transition to cascade is sharp, occurring just beyond the speed ratio which produces the minimum metered film thickness," that is, when $X_D = 0$. To support their data on the onset of cascade, Coyle et al. (1990) presented examples of finite-element computations of how the wetting line moves when the capillary number, Ca_A, and the speed ratio, V_M/V_A, are varied. These predictions are only qualitative, as they depend on the assumed value of θ_D and the slip coefficient near the wetting line. Figure 18 in their article and Figures 7.22 and 7.38 in Coyle's original thesis (1987) make this evident. Also, there is a discrepancy between the few results presented on X_D in their article and those in the original thesis. Figures 7.20 and 7.38 in the thesis and the corresponding Figures 7a and 18 in the article are out by a factor of two and $\sqrt{(R/2H_0)}$, respectively. Coyle et al. (1990) did not measure the movement of the wetting line and the dynamic contact angle, so their theoretical predictions could not be checked. More importantly they did not link their cascade air-entrainment findings to the hydrodynamic assistance of wetting.

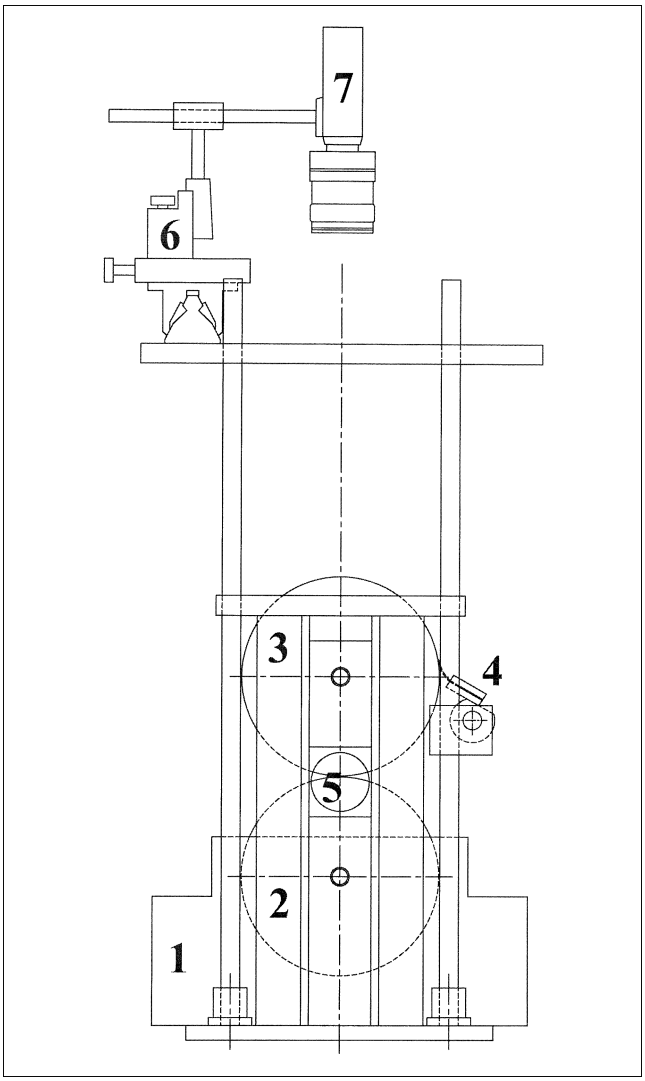

Figure 3. Experimental setup.

1—coating pan, 2—steel roller, 3—Perspex roller, 4—scraper blade, 5—side viewing window; 6—*xyz* moveable frame; 7—CCD camera with microlens.

In summary, this article presents the first data on the variation of X_D and θ_D with operating conditions in reverse-roll coating. The data were used to analyze dynamic wetting failure, and test the hydrodynamic assistance of wetting.

Experimental Setup

The experiments were carried out on a precision rig (Figure 3) with a steel applicator roller, chrome-plated and polished, and a metering roller made out of cast Perspex polished to give maximum transparency. The rollers were 0.19 m long$\times$0.20 m diameter with 0.1-micron surface finish. The difference between the shafts and the roller surfaces did not exceed 5 μm. The metering roller was wiped clean and dry by a plastic scraper to enable the formation of a dynamic wetting line. The gaps between the rollers were set by placing shims between the roller bearing blocks and checked using slip gauges. The rollers were driven independently by inverter-controlled AC geared motors via a combination of timing pulleys and belts. Initial calibration of the inverters provided accurate control of the roller speeds.

Visualization of the dynamic wetting region was achieved by focusing a CCD camera (Pulnix 765TM) coupled with a Canon Macro lens (50 mm, 1:3.5) directly above the Perspex metering roller and mounted on an accurately moveable *x-y-z* platform. The images captured by the camera were stored directly into a PC in bit-map format. The setup was properly calibrated by first determining the degree of magnification of the image captured using a photograph of a graticule placed in the nip between the rollers. The location of the center axis of the nip as viewed from the camera was determined by marking a line on the applicator steel roller and aligning it at its uppermost position. With both rollers stationary, an image was captured to give the position of the center line. With the rollers rotating during the coating experiments, images were collected to measure the position of the wetting line X_D with reference to this center line. The onset of air entrainment was observed visually from above the Perspex metering roller. At a fixed applicator roll speed, the metering roll speed was gradually increased until the onset of air entrainment could be observed. In order to reduce experimental errors, each data point was repeated at least four times. In spite of the relative crudeness of the experimental method, the discrepancies between individual and averaged data were always found to be less than $\pm 10\%$.

The coating bead was also observed from the side by illuminating the nip using a pulsed laser and focusing a long focal-length microscope at a point near the center of the nip. The images (Figure 4) collected were transmitted to a computerized image-analysis system to calculate the dynamic angle, θ_D, formed between the liquid and the dry surface of the roller. The chromed stainless steel applicator and metering rollers were used for the measurements of θ_D. The shiny surface of the chrome produced a mirror image of the meniscus region on the metering roller and this facilitated the determination of θ_D.

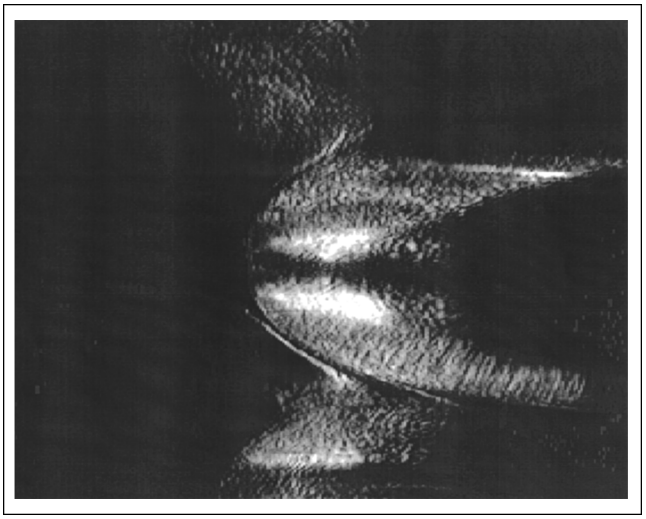

Figure 4. Image of meniscus and dynamic contact angle.

Note mirror image on metering roller.

During this experimental program, six lubricating oils were tested at gaps of 150, 250, 500, 750, and 1,000 microns and speed ratios ranging from 0.05 to 0.86. The viscosities of these fluids were measured in a Brabender Rheotron Rheometer and found to be Newtonian and at 20°C in the range 0.014–1.070 Pa·s ±5%. The surface tensions were measured using the pendent-drop method, and they were found to be 0.035 Nm^{-1} ±2%. The static-contact angles were measured by placing a 1-mm rod in a pool of the liquid and photographing the static meniscus formed using the setup described earlier. The angles were found to be 11° ± 1. For the purpose of comparison, the air entrainment in the plunging-tape flow was also measured with the test liquids using our laboratory dip coater described previously (Cohu and Benkreira, 1998).

Results and Discussion

With the combination of liquids, gaps, and roller speeds, 1,200 data points were gathered to establish (1) the coating window and, hence, the critical speed at which the metering roller begins to entrain or engulf air, and (2) the movement of X_D and θ_D with operating conditions. The observations are now presented and discussed in relation to previous findings. Here only the flooded case is considered, that is, the thickness of the film arriving at the nip is much larger than the gap. Note also that in this study we are not concerned with the ribbing instabilities that can occur downstream on the metered film (Coyle et al., 1990). Thus when we refer to a coating window, we are only considering the air-entrainment or engulfment limit.

Coating window

Figure 5 shows the coating window as a plot of the applicator capillary number, Ca_A vs. speed ratio, S. At dynamic wetting failure, the air was more engulfed in the form of large bubbles than entrained in the comparatively smaller bubbles we observed in plunging-tape experiments. Also, the classic V-shape wetting line, which could be seen in the plunging tape prior to air entrainment, was not observed in reverse-roll coating. Therefore, this air engulfment corresponds to the

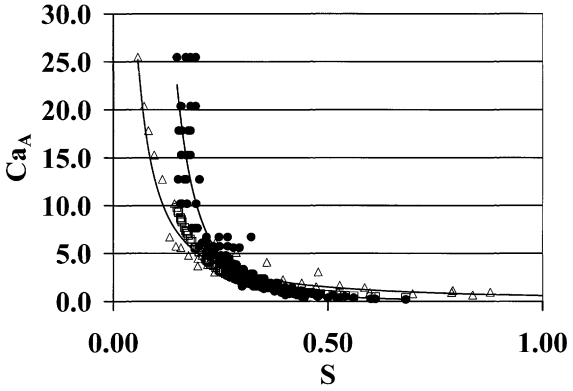

Figure 5. Coating window data in terms of Ca_A vs. S, and comparison with other data.

•: This work, Δ: plunging-tape data; □: Coyle's data.

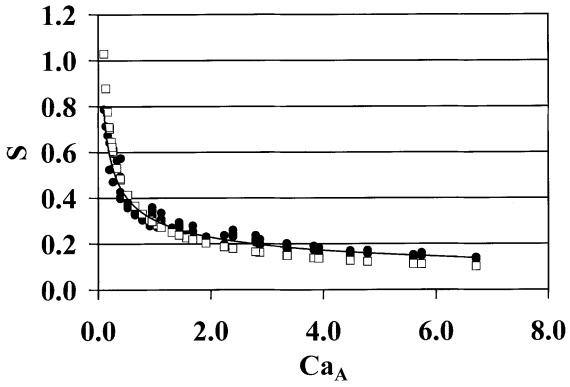

Figure 6. Comparison of our data (•) at $X_D = 0$ with those of Kang and Liu (1991) (□).

cascade instabilities described by Coyle et al. (1990). Here, the range of Ca_A was 0–25, much larger than that covered by Coyle et al. (1990), $Ca = 0$–4, and still only the cascade could be observed. We note from this curve that at a speed ratio less than 0.15, no air entrainment was observed up to $Ca_A =$ 25 (beyond this value, the nip in our arrangement could not be flooded). The data in Figure 5 compare well with the data of Coyle et al. (1990), and conform to their empirical correlation (Eq. 4). We also picked from our data the Ca_A vs. S points at which X_D is zero and compared them with the experimental correlation (Eq. 5) of Kang and Liu (1991). Here, as shown in Figure 6, the agreement is excellent. Both comparisons give confidence in the reliability of the measurements presented here.

Hydrodynamic assistance

For a given applicator roll speed, in Figure 5 we compare the cascade air-entrainment metering roll speeds with the *V*-type air-entrainment speeds measured with the same liquids that use a plunging tape. At low $Ca_A \leq 22 \sim 3$, cascade and plunging-tape air-entrainment speeds are similar. This suggests that the two forms of air entrainments may have *similarities* and they are not *completely different*, as stated by Coyle et al. (1990). When $Ca_A \geq 2 \sim 3$, the data clearly show that as the applicator Ca_A increases, the cascade speeds increase, becoming at $Ca_A = 25$ nearly four times as fast as the plunging-tape air-entrainment speeds. Therefore, although the two forms of air entrainment are *different*, the applicator roller in reverse-roll coating provides hydrodynamic assistance for wetting. This assistance is, however, not of the same order as that reported in curtain coating by Blake et al. (1994). There is also a threshold for hydrodynamic assistance to be effective in reverse-roll coating: the applicator capillary number Ca_A must be $\geq 2 \sim 3$, which corresponds to a speed ratio ≤ 0.30. This could explain why in practice reverse-roll coating is almost always run at low speed ratios. It also puts in perspective the limitations of computer-aided mathematical simulations for film-thickness calculations (Coyle et al., 1990), which set no bounds on the speed ratio. The data in Figure 5 can be rearranged to give the plot, in Figure 7, of a critical capillary number, $Ca_{\text{plunging or cascade}}$ vs. Ca_A for both the plunging tape and reverse-roll coating. This gives a better comparison, which

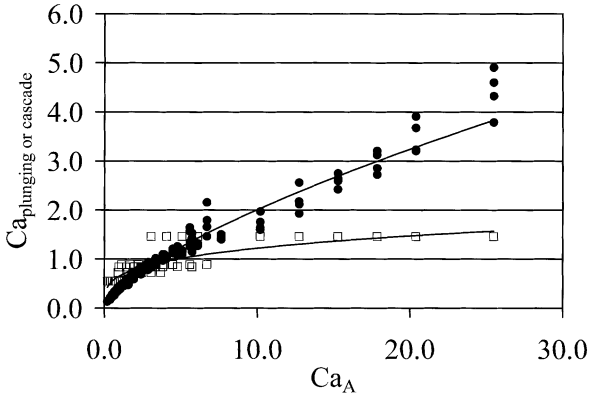

Figure 7. $Ca_{\text{plunging, cascade}}$ vs. Ca_A for reverse-roll coating (•) and plunging-tape flow (□).

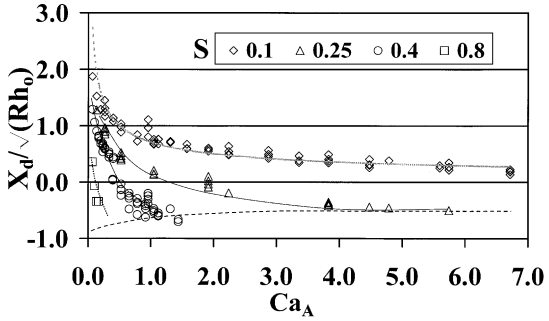

Figure 8. Data on the movement of $X_D/\sqrt{RH_0}$ with Ca_A and S.

Onset of cascade given by -----line.

brings out more clearly the hydrodynamic assistance of Ca_A. Of course, in the plunging-tape flow there is no Ca_A as such, but it can be used to define the corresponding Ca_{plunging} ($= Ca_A S$). Figure 6 shows that in the plunging-tape flow Ca_{plunging} is never more than 1.5, whereas in reverse-roll coating $Ca_{M,\text{cascade}}$ can be as high as 4 when $Ca_A = 25$. $Ca_{M,\text{cascade}}$ correlates with Ca_A with a coefficient of 0.985 as

$$Ca_{M,\text{cascade}} = 0.41 Ca_A^{0.69}. \tag{6}$$

This equation expresses the same results found by Coyle et al. (1990), which according to their Eq. 4, transforms to $Ca_{M,\text{cascade}} = 0.43 Ca^{0.54}$.

In the preceding analysis the gap effect was not considered. We now discuss the individual contribution of the gap, applicator speed, and viscosity to this hydrodynamic assistance. The experimental results on $V_{M,\text{cascade}}$ correlate with a confidence limit of $\pm 7\%$ and $\pm 3\%$, respectively, in the form

$$V_{M,\text{cascade}} = 0.24 H_0^{0.03} V_A^{0.81} \mu^{-0.19} \tag{7a}$$

$$V_{M,\text{cascade}} = 0.20 H_0^{0.04} V_A^{0.69} \mu^{-0.28} \tag{7b}$$

These correlations are remarkably similar to Blake et al. (1994) theoretical and experimental Eqs. 2 and 3. They explain that the contribution of the applicator roller to hydrodynamic assistance of wetting is similar to the contribution of the impinging curtain flow. The gap effect in reverse-roll coating is small because it does not assist in pinning the wetting line. In comparison with curtain coating, however, the air-engulfment speeds observed in reverse-roll coating are smaller. This is because the fluid in the gap splits and turns, and the impinging part of the applicator roll speed V_A is small compared with the curtain speed U. Note also that Eq. 6 and 7 are in agreement, as expected.

Movement of X_D with operating conditions

Figure 8 displays the data up to the conditions of air engulfment, which occurs well inside the nip and for a range of positions. It does not occur only when $X_D = 0$, as was inferred by the experimental observations of Coyle et al. (1990) and their proposed link with the correlation of Kang and Liu (1991) for the minimum metered film thickness (Eq. 5).

At constant S, increasing Ca_A pushes X_D inside the nip. Also X_D moves in at constant Ca_A as S is increased. At all speed ratios, the effect of Ca_A is particularly strong when $Ca_A < 1$. For $Ca_A > 4$ and $S < 0.25$, the X_D values become almost independent of Ca_A. Speed ratios of about 0.2 are sufficient to pull X_D beyond the minimum gap position. This again explains why in practice reverse-roll coating is almost always run at low speed ratios. These observations are consistent with those made earlier about the role of the applicator roller.

In order to assess the movement of X_D with operating conditions, a reference point is required. The normal reference position, $X_{D,\text{ref}}$, occurs when the metering roll is stationary. Using the appropriate scale, we can correlate these data as $X_{D,\text{ref}}/\sqrt{RH}_0 = aCa_A^b$. When we introduce the effect of the metering roller, the speed ratio, S, is the additional parameter. We can account for the movement of X_D in relation to $X_{D,\text{ref}}$ by modifying the form of the preceding equation as $(X_{D,ref} - X_D)/\sqrt{RH}_0 = cCa_A^d S^e$. Examination of the data suggests a linear correlation with the speed ratio, that is $e = 1$. The preceding equations when combined should reduce to $X_D/\sqrt{RH}_0 = aCa_A^b - cCa_A^d S$. Taking all the data, we could correlate them according to the previous equation with a 0.96 coefficient of correlation as

$$X_D/\sqrt{RH}_0 = \left[1.189\ Ca_A^{-0.229}\right] - \left[3.902 Ca_A^{0.1986}\right] S. \tag{8}$$

No comparison with theoretical predictions can be made because the few published results depend on the assumed value of the contact angle and the slip coefficient (Coyle's original thesis, 1990). Therefore, it will be useful to use various contact angles and slip coefficients to generate complete sets of predicted $X_D/\sqrt{RH}_0$ from simulations with a range of Ca_A, S, and H_0/R and compare them with the present data.

Evolution of θ_D with operating conditions

It must be noted that θ_D values very near 180° could not be recorded in these experiments. This is because the onset of air entrainment in reverse-roll coating is in the form of a cascade, whose occurrence is sharp and associated more with

the movement of X_D inside the nip rather than the gradual increase of θ_D toward 180°. Figure 1 displays all the data from this study. Although there is scatter in the data, the figure shows that the dynamic contact angle data fall broadly on a single curve, $\theta_D = f\ (Ca_M)$ where $Ca_M = \mu V_M/\sigma$. Thus, as expected, the metering capillary number is the main control parameter, with the other variables (the gap and the applicator roll speed) having secondary effects. When these secondary effects were lumped into $Re_A = \rho V_A\ H_0/\mu$, the data could be correlated with a correlation coefficient of 98% as

$$\theta_D = 240.37 Ca_M^{0.284} Re_A^{-0.092} \tag{9a}$$

where Re_A has a reducing effect that is consistent with the proposition that hydrodynamic assist is present, albeit small. It must be noted that, taken alone, the exponent of Re_A can be misleading. In our experiments, Re_A ranged from 0 to 60, and Ca_M ranged from about 0.01 to 1. Therefore θ_D will be quite sensitive to Re_A when Ca_M is small and Re_A large. This is consistent with the concept of hydrodynamic assistance for this flow. At a low metering roller speed or Ca_M, the effect of high applicator speed or Re_A is to reduce θ_D in comparison with the plunging-tape where there is no assisting flow. Figure 1 highlights this point by comparing our findings with the plunging-tape data of other workers. The values are broadly comparable. At $Ca_M > 0.1$, our data converge with others, but at $Ca_M < 0.1$, they begin to diverge, showing relatively smaller θ_D. If Re_A is removed in the data correlation, we obtain a simpler but less mechanism descriptive equation

$$\theta_D = 241.07 Ca_M^{0.295} \tag{9b}$$

Conclusions

The data on cascade speeds, the position of dynamic contact line, and the angle it forms with the substrate collected in this experimental program complete the specifications of the boundary conditions and operating bounds of reverse-roll coating. These can now be utilized to obtain accurate flow predictions. The data all point to the occurrence of hydrodynamic assistance of wetting in reverse-roll coating, which is similar to curtain coating. There is a threshold, however: Ca_A must be greater than about $2 \sim 3$. Finally, noting that when hydrodynamic assistance was not prevailing, the cascade speeds in reverse-roll coating were similar to the V-type speed in the plunging tape flow, the study concludes that these two types of air entrainment may not be as different as reported previously.

Acknowledgments

The author acknowledges the financial support of The UK Research Council under EPSRC Grant, GR/L96493. The data reported here were collected by Dr. R. Patel, who was the postdoctoral assistant employed in this project.

Notation

Ca_A, Ca_M = applicator, metering roller capillary number ($\mu V_A/\sigma$, $\mu V_M/\sigma$)
Ca_{plunging} = plunging flow critical capillary number ($\mu V^*_{\text{plunging}}/\sigma$)
H_0 = metering gap, m
S = roller speed ratio (V_M/V_A)
R = roller radius
Re_A = applicator roller Reynolds number ($\rho V_A\ H_0/\mu$)
U = impingement speed in curtain coating flow, m/s
V = plunging tape speed, m/s
V_A, V_M = applicator, metering roll speed, m/s
V^*_{plunging} = air-entrainment speed in plunging flow, m/s
V^*_{curtain} = maximum air-entrainment speed in curtain coating, m/s
$V_{M,\ \text{cascade}}$ = air-engulfment speed in reverse-roll coating, m/s
X_D = dynamic wetting line position, m
θ_S, θ_D = static and dynamic contact angle, deg
μ, ρ, σ = fluid viscosity (Pa·s), density (kg/m^3), surface tension (kg/s^2)

Literature Cited

Blake, T. D., A. Clarke, and K. J. Ruschak, "Hydrodynamic Assist of Dynamic Wetting," *AIChE J.*, **40**, 229 (1994).

Blake, T. D., and J. M. Haynes, "Kinetics of Liquid/Liquid Displacement," *J. Colloid Interf. Sci.*, **30**(3), 421 (1969).

Blake, T. D., and K. J. Ruschak, "Wetting Static and Dynamic Contact Lines," *Liquid Film Coating*, S. F. Kistler and P. M. Schweizer, eds., Chapman & Hall, London, p. 65 (1997).

Bracke, M. F., F. De Voeght, and P. Joos, "The Kinetics of Wetting: The Dynamic Contact Angle," *Prog. Colloid Poly. Sci.*, **79**, 142 (1989).

Burley R., and R. P. S Jolly, "Entrainment of Air into Liquids by a High Speed Continuous Solid Surface," *Chem. Eng. Sci.*, **39**, 1357 (1984).

Burley, R., and B. S. Kennedy, "An Experimental Study of Air Entrainment at a Solid-Liquid-Gas Interface," *Chem. Eng. Sci.*, **31**, 901 (1976).

Buonoplane, R. A., E. B. Gutoff, and M.M.T. Rimore, "Effect of Plunging Tape Surface Properties on Air Entrainment Velocity," *AIChE J.*, **32**, 682 (1986).

Cohu, O., and H. Benkreira, "Air Entrainment in Angled Dip Coating," *Chem. Eng. Sci.*, **53**(3), 533 (1998).

Coyle, D. J., "The Fluid Mechanics of Roll Coating: Steady Flows, Stability, and Rheology," PhD Thesis, Univ. of Minnesota, Minneapolis, (1984).

Coyle, D. J., C. W. Macosko, and L. E. Scriven, "The Fluid Dynamics of Reverse Roll Coating," *AIChE J.*, **36**, 161 (1990).

Coyle, D. J., "Knife and Roll Coating," *Liquid Film Coating*, S. F. Kistler and P. M. Schweizer, eds., Chapman & Hall, London, p. 539 (1997).

Deryagin, B. M., and S. M. Levi, *Film Coating Theory*, Focal Press, London, (1964).

Dussan, V., "On the Spreading of Liquids on Solid Surfaces: Static and Dynamic Contact Angles," *Ann. Rev. Fluid Mech.*, **11**, 371 (1979).

Esmail, M. N., and M. T. Ghannam, "Air Entrainment and Dynamic Contact Angles in Hydrodynamics of Liquid Coating," *Can. J. Chem. Eng.*, **68**, 197 (1990).

Gutoff, E. B., and C. E. Kendrick, "Dynamic Contact Angles," *AIChE J.*, **28**, 459 (1982).

Hoffman, R. L., "A Study of the Advancing Interface 1. Interface Shape in Liquid-Gas Systems," *J. Colloid Interf. Sci.*, **50**(2), 228 (1975).

Inverarity G., "Dynamic Wetting of Glass Fibre and Polymer Fibre," *Br. Poly. J.*, **1**, 245 (1969).

Kang, Y. T., and T. J. Liu, "Minimum Film Thickness in Reverse Roll Coating," *Chem. Eng. Sci.*, **46**(11), 2958 (1991).

Perry, R. T., "Fluid Mechanics of Entrainment through Liquid-Liquid and Liquid-Solid Junctures," PhD Thesis, Univ. of Minnesota, Minneapolis, (1967).

Rillaerts, E., and P. Joos, "The Dynamic Contact Angle," *Chem. Eng. Sci.*, **35**, 883 (1980).

Schwartz, A. M. and S. B. Tejada, "Studies of Dynamic Contact Angles on Solids," *J. Colloid Interf. Sci.*, **38**, 359 (1972).

Manuscript received Dec. 19, 2000, and revision received July 11, 2001.